# Designing A Shock Tunnel To Enable High Enthalpy Experimental Investigation Of Hypersonic Flows.

Sumukh Peddada

A dissertationsubmitted in partial fulfillment of the
requirements for the degree of

Masters in Aeronautics and Astronautics

University of Washington

2024

Committee:

Owen J. H. Williams

Carl Knowlen

Program Authorized to Offer Degree:
Aeronautics and Astronuautics

University of Washington

**Abstract**

Designing A Shock Tunnel To Enable High Enthalpy Experimental Investigation Of Hypersonic Flows.

Sumukh Peddada

Chair of the Supervisory Committee:

This study presents the design and analysis of a shock tunnel facility, utilizing existing high-pressure pipes within the UWAA department. The research aims to elucidate the trade-offs between Reynolds number, enthalpy, and test time across a range of configurations. The methodology involves using the WISTL shock tube code from the University of Wisconsin, integrated with an in-house nozzle solving code to design and model a reflected shock tunnel. The setup features a driver length of 12 $ft$ and a driven length of 56 $ft$ with a diameter of 7 $in$, achieving steady-state test durations ranging from 3 to 16 $ms$. This configuration enables exploration of Reynolds numbers from $10^6$ - $10^8$ $m^-1$ and enthalpy conditions from 0.3 - 1.6 $MJ/kg$. A comparative analysis with a Ludweig tube configuration, using the same pipe sections, demonstrates the shock tunnel's capability to handle high enthalpy at higher Mach numbers without issues, offering greater flexibility. The results reveal stable stagnation conditions with minimal pressure and temperature fluctuation with changes in length but high sensitivity to driver and driven pressures. A Mach Number in the range 6 - 8 with the current test section size of 0.3m is identified as striking a reasonable balance between various parameters. In conclusion, the designed shock tunnel facility demonstrates remarkable flexibility and robust performance over test conditions and showcasing its potential for advancing research in hypersonic flow.

## TABLE OF CONTENTS

## LIST OF FIGURES

## NOMENCLATURE

*Variables*

| | |
|---|---|
| $A_t$ | Nozzle Throat Area |
| $a$ | Speed of Sound |
| $C_p$ | Specific Heat at Constant Pressure |
| $C_v$ | Specific Heat at Constant Volume |
| $M$ | Mach Number |
| $P$ | Pressure |
| $P_0$ | Stagnation Pressure |
| $R$ | Gas Constant |
| $T$ | Temperature |
| $T_0$ | Stagnation Temperature |
| $M_{up}$ | Upstream Mach |
| $A_{tube}$ | Area of driven tube |
| $T_{static}$ | Static Temperature |
| $P0$ | Stagnation Pressure - Shocktube |
| $T0$ | Stagnation Temperature - Shocktube |
| $P_4$ or $P_{0,4}$ | Driver Pressure - Shocktube |
| $P_1$ | Driven Pressure - Shocktube |
| $P0, test$ | Stagnation Pressure of Test Section - Shocktube |
| $T0, test$ | Stagnation Temperature of Test Section |
| $Re$ | Reynolds Number |
| $H_0$ | Enthalpy |
| $D_{test}$ | Test Section Diameter |
| $D_t$ | Throat Diameter |
| $t_c$ | Test time |

## ACKNOWLEDGMENTS

*I would like to express my sincere gratitude to my Professor, Owen Williams for his constant support and encouragement throughout my Master's research and thesis writing journey. Professor Williams's guidance was invaluable, particularly his insightful feedback on research direction and encouragement during challenging moments. He has greatly motivated me to delve deeper into my research and been understanding and motivated our cohort to expand our horizon. I am deeply grateful to Marvin for his exceptional work in the UW Ludwieg Tube Design, including 3D modeling, which played a pivotal role in visualizing and refining the design of the shock tubes in this study. His technical proficiency and attention to detail significantly contributed to the accuracy and realism of our simulations. I would also like to thank my colleagues who provided valuable guidance during the project and helped me troubleshoot various problems. Lastly, I would like to thank my parents who provided constant support in many forms.*

## DEDICATION

to my Family and Friends

# Chapter 1

# INTRODUCTION

## *1.1 Motivation*

Hypersonic flows are integral to the advancement of many aerospace technologies, including hypersonic vehicles, spacecraft reentry, hypersonic weapons, and high-speed air travel. Shock tunnels serve as crucial tools for simulating extreme hypersonic flight conditions. Noteworthy facilities such as NASA HYPULSE [8], High Energy Shock Tunnel Göttingen (HEG) [20], CUBRC LENS [21] and Caltech T5 [34] play pivotal roles, enabling the study and comparison in a controlled environment, leading to significant advancements in our understanding. The unique setup of shock tunnels involves the release of high-pressure driver gas into low-pressure driven gas through a ruptured diaphragm. By incorporating a nozzle to the setup, we can precisely control and manipulate the flow to achieve specific Mach number and pressure conditions more closely resembling flight. The design of a shock tunnel necessitates meticulous consideration of various factors, including dimensions, pressures, temperatures, and Mach numbers, with the ultimate goal of achieving conditions that are competitive with other facilities. In this thesis, the use of the available shock tube in the Aeronautics and Astronautics department will be used for the construction of a reflected shock tunnel (RST) to explore the trade-offs between enthalpy ($H_0$), $Re$, test section Mach number, and test time, then compare the designed capabilities with other hypersonic shock tunnels.

## *1.2 Literature Review*

Hypersonic testing facilities are crucial for simulating the extreme conditions experienced by vehicles traveling at high speeds, with each type of facility offering unique advantages and facing specific challenges. Reflected shock tunnels are designed to create high-pressure, high-temperature test conditions by reflecting shock waves back through the test section.

These tunnels typically consist of two pipes, the driver and driven sections, with a nozzle attached downstream of the shock tube. This is achieved by generating a shock wave in a driver section, which then travels through a test section and is reflected off a downstream surface. The reflected shock wave interacts with the incoming flow, creating the desired high-pressure and high-temperature conditions. Reflected shock tunnels such as the Stevens Shock Tunnel [33] work on this principle

There are many ways to operate such a facility. The HyperTERP Facility [5] uses gas tailoring to halt the contact surface, preventing shockwave interference and increasing test times. However, adjusting the gas mixture can increase Reynolds numbers at the expense of enthalpy. Some reflected shock tunnels, like the T6 Stalker Tunnel [10], incorporate a free-piston driver with modified barrels, allowing various operating modes such as shock tube, reflected shock tunnel, or expansion tunnel. However, larger diameters can reduce performance by limiting maximum shock speed due to lower pressure and temperature downstream of the nozzle. This operation also requires precise control over driver gas composition and flow rates, which can be challenging to maintain. Detonation drivers, such as HYPULSE [38], JF12 [23], and the TH2 Tunnel [37], leverage combustion dynamics to generate high-speed flows. Helium is often used as the driver gas due to its low molecular weight, which allows for high flow velocities at lower pressures. While detonation drivers offer high Reynolds numbers and precise control over flow conditions, they can be challenging to operate and require specialized expertise to maintain.

Larger facilities, including the CUBRC LENS [7], T4 Tunnel [35], HEG [20], and T5 CALTECH Tunnel [34], work with larger test sections and higher driver pressures. These conditions produce high enthalpies and Reynolds numbers, eliminating driver gas contamination and ensuring accurate flow measurements. However, maintenance of larger facilities can be more complex and costly, requiring extensive calibration and downtime for repairs.

In addition to reflected shock tunnels, there are other facilities used for high speed flow research. Continuous facilities, such as AEDC Tunnel B and AEDC Tunnel C [28], provide a steady flow of high-speed gas for comparatively long-duration experiments. They typically include a high-pressure storage vessel, a flow control system, and a test section. Blowdown facilities, such as AEDC Tunnel 9 [26], are ideal for studying transient phenomena and

are commonly used for aerodynamic testing of aerospace components. Gun tunnels, like Longshot and VKI [17], accelerate projectiles to high speeds using a compressed gas gun, generating high-speed flows in the test section upon impact. They consist of a launch tube, a projectile, and a test section. Gun tunnels are valuable for studying high-speed impact phenomena and material behavior under extreme conditions. Adiabatic compression units, such as AT-303 [15], rapidly compress gas using mechanical means, creating high-speed flow conditions. They typically include a compression chamber, a gas storage tank, and a test section. Adiabatic compression units are suitable for studying high-speed combustion and gas dynamics.

Expansion tunnels, such as MHExT [1], HET [4], and Stanford University [13], use a high-pressure reservoir to generate high-speed flows through a converging-diverging nozzle. They consist of a driver section, a nozzle, and a test section. Expansion tunnels are cost-effective and suitable for a wide range of aerodynamic testing applications.

The diverse range of hypersonic testing facilities offers researchers valuable tools for studying high-speed flows and advancing the understanding of hypersonic aerodynamics and propulsion. Each type of facility has its unique capabilities and limitations, making them suitable for different aspects of hypersonic research and development.

### *1.3 Approach and Objectives*

In this work, the capabilities of a shock tunnel are explored, basing the geometry on pipes that are already available. The work focusses on exploring the trade-offs between test time, Reynolds number, enthalpy, and Mach number. Our methodology begins with utilizing the WISTL Code [6] to determine the range of conditions at the downstream end of the driven tube, computing stagnation pressures ($P_0$) and temperatures ($T_0$) with air as the working gas and both driver and driven tubes filled at 300 K. Subsequently, we employ an in-house nozzle code to expand these stagnation conditions to high Mach numbers, exploring the trade-offs between Mach number and nozzle test section size. Our paramount focus is the design and optimization of tunnel geometry and flow conditions, including Mach numbers and test section sizes, to discern the intricate trade-offs between test time, Reynolds number ($Re$), and stagnation enthalpy ($H_0$). We draw on seminal works such as Chun-Min Wang's

Table 1.1: Summary of the Reflected Shock Tunnel Facilities

| **Tunnel** | **Operation Type** | **Mach** | $H_0$ $(MJ/kg)$ | $Re$ $(\times 10^6\,\mathbf{m}^{-1})$ | **Source** |
|---|---|---|---|---|---|
| Stevens | Driver-Driven | 5.8-6 | 1.5 | 0.35-8.1 | [33] |
| HyperTERP | Driver-Driven | 6 | 1.4, 0.7 | 5.3 | [5], [30] |
| Sandia | Free Piston Driver | 8-9 | 4.6 | 1-4 | [25] |
| T6 Stalker | Free Piston Driver | 7 | 2.4 | 10 | [10] |
| CUBRC-LENS | Driver-Driven | 6.5-8.2 | High | 0.055-1.6 | [7] |
| HEG | Free Piston Driver | 6 -10 | 1.5 - 22 | 0.2 - 133 | [19] |
| T5 Tunnel | Free Piston Driver | 5.2 | 25 | 2 - 6 | [22] |
| HYPULSE | Dual Mode | 12 - 25 | High | High | [38] |
| JF12 | Detonation Driver | 5 - 9 | - | - | |
| TH2 | Free-Piston/Detonation Driver | 6.6 - 12.1 | 0.8 - 16.5 | 14.1 | [37] |
| T4 Tunnel | Free-Piston Driver | 4-10 | 2.5-15 | - | [35] |

analysis of transonic flow in supersonic Ludwieg wind tunnels [39], and feasibility studies by John W. Davis et al. on high Reynolds number tube wind tunnels at NASA [12], which provide foundational insights and benchmarks for our research.

# Chapter 2

# METHODOLOGY

The design process involves several key steps to develop an effective shock tube using these UW pipes: Ensuring the driver tube can handle high-pressure gas that is essential to contain the high-pressure gas before the shock wave is generated, to prevent premature failure and ensure safety; choosing 12-foot and 56-foot lengths for the driver and driven sections to provide sufficient distance for shock wave development and interaction with the test gas; using the 7-inch inner diameter to accommodate the necessary volume of gas and maintain appropriate flow dynamics. To begin with, we observe the tradeoffs with pressures lengths and temperatures for shock tube portion. With nozzle calculations, we explore the tradeoffs of test section size and Mach number and the influence this has on the Reynolds number (Re) and stagnation enthalpy (H0). We assume a perfect gas even at higher temperature scenarios. The gas filled in the shock tube is set to ambient temperature (300 K). We use a lossless nozzle and air for our potential design.

## *2.1 Available shock tube pipes*

The geometric configuration of the UW shock tube, using the set of pipes we currently have in the historic AA department, is a crucial factor in its design, directly influencing performance and experimental outcomes. The driver section, with a pressure range of 100 psi to 5000 psi, and the driven section, with a pressure range from 0.5 atm (7.5 psi) to 50 atm (750 psi), are rated for these pressures based on specifications. These pipes have an inner diameters of 7 inches, driver tube with an outer diameter of 14 inches and driven tube with an outer diameter of 10 inches. The material employed is molybdenum. Lengths of 12 feet for the driver section and 56 feet for the driven section. Figure 2.1 and Table 2.3 enhance comprehension and facilitate the analysis of a shock tube. Each component's dimensions, including the lengths, diameters, and pressure ratings of the driver tube, driven

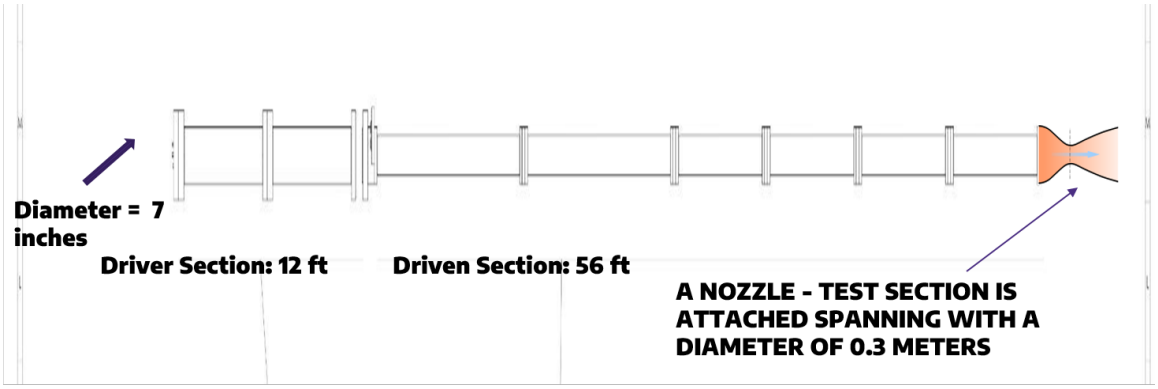


Figure 2.1: UW Shock Tunnel Drawing (length not to scale).

tube, and interaction region, are carefully considered to ensure optimal functionality.

## *2.2 Design process for reflected shock tunnel (RST)*

This involves attaching a nozzle to the initial shock tube setup. This nozzle expands the flow, converting the shock tube into a functional shock tunnel. The shock tube calculation provides crucial outputs like Stagnation Pressure ($P_{0,5}$), Stagnation Temperature ($T_{0,5}$), and Test Time ($t_c$). These outputs define the initial conditions for the nozzle calculation, which provides test section pressure ($P_{0,test}$),test section temperature ($T_{0,test}$), Reynolds number $Re$, enthlapy $H_0$ and static temperature ($T_{static}$) after expansion. The shock tube $x$-$t$ diagram as shown in figure 2.2 illustrates key regions like the shock wave, contact surface, and expansion wave, with variables defined for each region. This sequential approach, starting with the shock tube calculation and then using its outputs for the nozzle calculation, ensures that the RST achieves the desired hypersonic flow conditions for our design.

### *2.2.1 Functionality*

The utilization of the WISTL Code [29], is instrumental in generating x-t diagrams, crucial for understanding shock tube dynamics. This process involves executing a second-order finite volume code, employing the Muscl-Hancock method alongside an exact Riemann solver. We are empowered to execute .exe files by providing an input document laden with

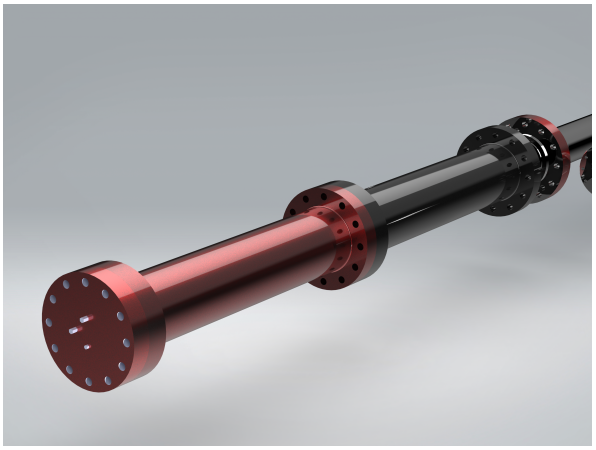

Table 2.1: Driver Section

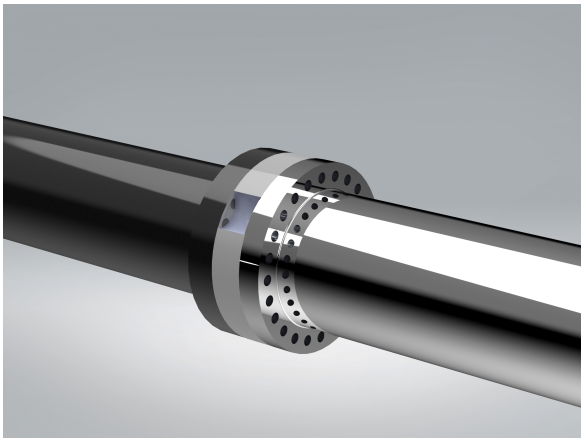

Table 2.2: Driven Section

Table 2.3: Essential components for assembling a shock tube

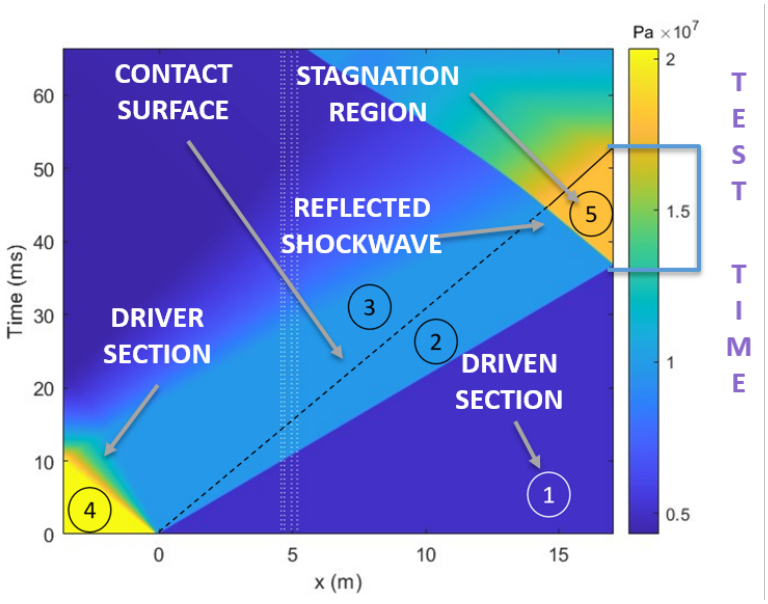


Figure 2.2: An Example x-t

various parameters tailored to specific shock tube and gas combinations. These parameters encompass critical factors such as tube length, diaphragm and interface locations, as well as pressures, temperatures, and gas properties. By adjusting these parameters to meet our design and criteria requirements, we initiate simulations, thereby yielding essential data files for further analysis. Subsequently, these data files undergo processing via a MATLAB script, facilitating the creation of vivid color and contour plots. Notably, the MATLAB script enhances visualization by accurately tracking diaphragm and interface locations on the plots. Figure 2.2 aptly demonstrates the culmination of this process, showcasing the x-t diagrams generated by the WISTL software [29].

*Example output*

The x-t diagrams using the WISTL Code [29], a 1-D gas dynamics based solver assuming the ideal gas equations of state, presented in Figure 2.3 illustrate the overall dynamics of the flow and the critical scenario downstream of the shock tube, emphasizing the region of stagnation conditions. This setup corresponds to a full-length shock tube configuration, where the driver and driven sections are connected with a diaphragm in between. This code serves as a valuable tool in shock tube experiments, providing a visual representation of shock and rarefaction waves within the tube. It illustrates critical events such as the interaction of the reflected shock with the interface and the timing of the rarefaction from the driver reaching the interface before further interaction. Figure 2.2 illustrates the speicfic regions duing a shock tube process. Initially, the shock tube is divided into two sections by a diaphragm. Region 4, known as the driver gas region, contains high-pressure gas that drives the shock wave. Region 1, the driven gas region, contains gas at rest initially, which will be accelerated by the shock wave. When the experiment begins, the diaphragm ruptures, allowing the high-pressure driver gas to rapidly expand into the low-pressure driven section. This expansion creates a high-velocity shock wave that propagates down the tube. As the shock wave moves down the tube, it compresses the gas in front of it, creating a region of high pressure and temperature behind the shock front. Regions 2 and 3 are located on either side of the contact surface, which is the interface between the driver and driven gases. Across

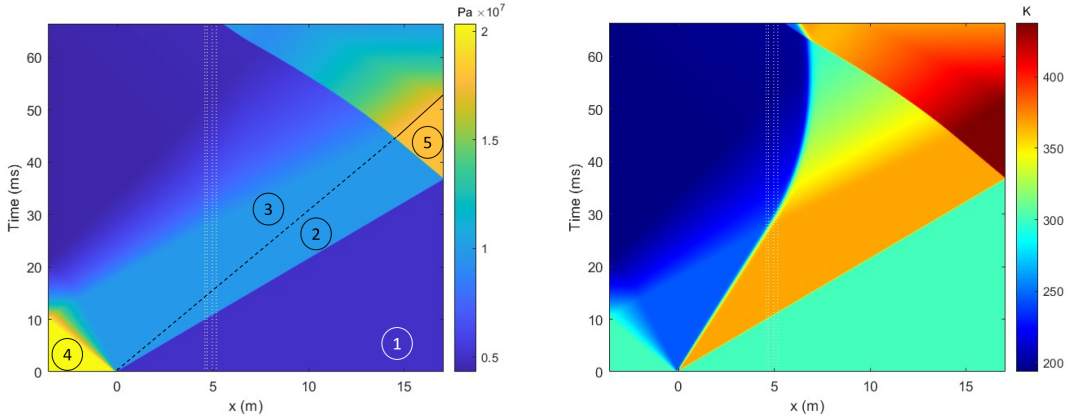


(a) Pressure (b) Temperature

Figure 2.3: $(P_4) = 3000\ psi \mid (P_1) = 750\ psi$ [29]

this surface, the pressures and velocities remain constant. When the shock wave reaches the end of the tube, it reflects back towards the diaphragm. This reflection creates a region of high pressure and temperature known as the stagnation region **(Region 5)**, where we attach a nozzle to extract test conditions to develop a shock tunnel. To determine the test times accurately, it is essential to record the duration of this stagnation period precisely. This involves measuring the time interval between the rupture of the diaphragm and the onset of interaction with the contact surface.

For the purposes of discussion in this section, we consider an example shock tube model with a driver pressure $(P_4)$ of 3000 $psi$ and a driven pressure $(P_1)$ of approximately 50 $atm$. This example scenario enables us to delve into the dynamics of shock tube experiments and analyze the behavior of shock and rarefaction waves under these specific pressure conditions. Our analysis involves calculating the shock tube conditions for various pressures and lengths, followed by the attachment of a nozzle. This approach allows us to examine the behavior of the shock tube and subsequent flow dynamics in detail, providing a comprehensive understanding of the setup and its implications. To achieve these shock tube conditions for a range of configurations, including short to long sections and different pressures, we utilize the WSITL code [29] as mentioned previously.

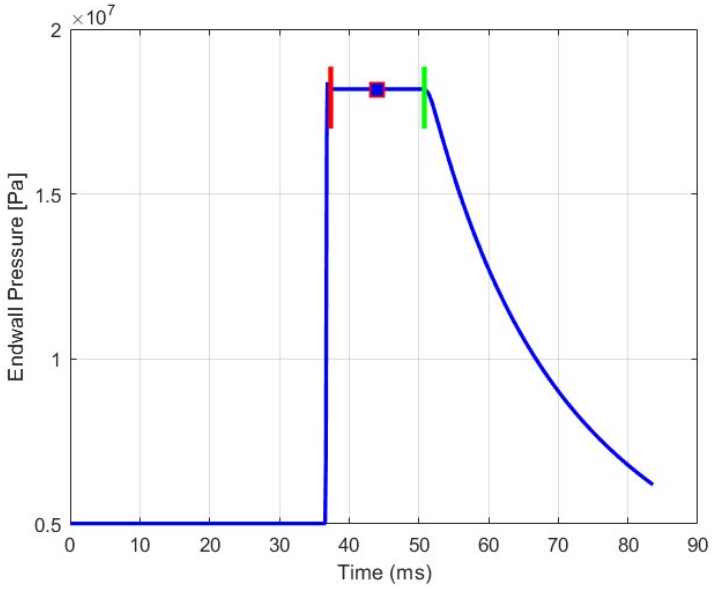


Figure 2.4: Using data from Figure of 2.3, $(P_4) = 3000\ psi \mid (P_1) = 750\ psi$

### *2.2.2 Extraction and Analysis of Stagnation Conditions and Test Times in a Shock Tube*

Shock tube test time refers to the duration of a shock tube experiment, specifically focusing on capturing the duration of the observed stagnation condition during the test. It encompasses the period from the reflection of the shockwave, which pressurizes and heats the gases at the test section, to the interaction of the shockwave with the expansion waves or the contact surfaces. According to Figure 2.4, we typically seek points in the signal where the pressure either tapers off or changes rapidly. This process involves the code examining the signal to identify regions along the end wall of the shocktube where the pressure or temperature remains relatively constant at the downstream end of the driven pipe (stagnation region). For instance, in a pressure signal, the aim is to locate a region where the pressure sharply rises downstream of the tube and then stabilizes, indicating the arrival of the shockwave at the end section and marking the interaction of waves of interest. The code we develop performs several steps to identify regions of constant pressure at the end of a shock tube, which are crucial for determining test times and analyzing the stagnation region.

The test time region is identified as the time within which the pressure is within a percentage $\epsilon$ of the maximum pressure, $P_{max}$, such that,

$$\delta P = P_{\max} \times \frac{\epsilon}{100}$$

where $\delta P$ is the allowable deviation in pressure from the maximum.

We identify a region of constant pressure if the difference between each pressure value $P_i$ and the maximum pressure $P_{\max}$ is less than or equal to a specified tolerance $\delta P$, considering both increases and decreases in pressure:

$$|P_{\max} - P_i| \leq \delta P$$

.

A threshold $\epsilon$ of 5% was used for all cases. This calculated tolerance is then used to determine regions where the pressure change between points is minimal and considered "constant" within this tolerance. If no constant pressure regions are found within the given tolerance, the test conditions are considered not valid. This process determines the maximum pressure values within the identified constant pressure region to understand the start and end point of the pressures which is where the pressure starts to increase/decrease after being constant. This process ensures accurate identification of the stagnation region. This method operates by extracting the pressure data from the WISTL Code [29]. These red and green lines as depicted in Figure 2.4 indicate the start and end of the stagnation region downstream. The difference between these two points is calculated, defining the test time. Since the pressure is constant in Region 5, we select a mean point indicative of the stagnation value. The main objective of this code is to calculate and extract these stagnation values and test times for multiple cases and feed them into the nozzle code for further analysis of a shock tunnel. As shown in Figure 2.5, even in rare instances of non-ideal behavior, the thresholds effectively detect a valid test time.

### *2.3 Expanding Stagnation Conditions through a Nozzle*

When a shock tube experiment reaches the stagnation region (Region 5), as shown in Figure 2.3, we expand the these test conditions through a lossless nozzle at different Mach numbers

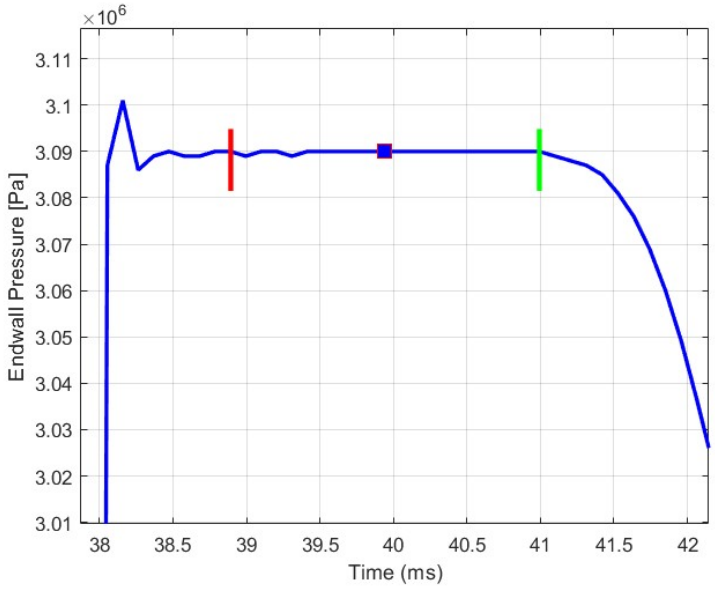


Figure 2.5: Example for an Off-Nominal Case for Endwall Pressure vs Test Time

(area ratios). Such calculations are the same as for a Ludweig tube, and so the operating principle of these facilities and their calculations is outlined below.

### *2.3.1 The Ludweig Tube in Focus: An Overview*

The Ludwieg tube utilized in our research comprises of our driver ( in our case driven) section of 56 $ft$ and the nozzle test section of 0.3 meters, involves the sudden release of high-pressure gas from a reservoir into a larger, lower-pressure tube. This rapid expansion generates a shock wave that travels down the tube, akin to a shock tube. Figure 2.6 [8] provides a schematic of a hypersonic Ludwieg tube. When the diaphragm ruptures, the expansion wave accelerates the high-pressure gas, generating a shock wave and contact surface in the nozzle and test section downstream. The test time is defined as the duration during which the expansion fans travel upstream of the charge tube, reflect towards the nozzle throat, and maintain steady flow. The shock wave propagates through the nozzles, resulting in high pressures and temperatures. As we aim to expand our understanding of this flow to produce a tunnel, the code for the Ludweig Tube becomes valuable as it

operates on the same principles since we use the same nozzle test section to expand the flow for the shock tunnel. This code, to be discussed in the following section, is derived from the set equations that will be outlined. Extensive research has been conducted on the UW Ludweig Tube [27], enabling a comparative analysis between the Ludweig Tube and our Shock Tunnel. Subsequent sections will delve into this comparison, elucidating the differences in performance and the significance of various parameters. We aim to integrate this code into our workflow to expand the stagnation conditions through the nozzle. In our workflow, we begin by acquiring stagnation values using the WISTL framework [29] which we refined and upgraded to enhance its functionality. The **shocktube** stagnation values serve as inputs for the Ludwieg Tube Code [27], along with fundamental inputs like Mach number and test section size. Through iterative refinement of these calculations, our objective is to identify the most suitable case for designing the facility, considering factors such as nozzle geometry and gas properties. This iterative (different test cases) approach is essential for optimizing the design to achieve the desired flow conditions and performance levels, ensuring the efficiency and effectiveness of our facility.

### *2.3.2 Design Criteria to set the Flow*

The nozzle is typically designed as a converging-diverging nozzle, also known as a de Laval nozzle. The expansion ratio of the nozzle, defined as the ratio of the exit area to the throat area, is carefully selected to achieve the desired Mach number in the test section. A higher expansion ratio results in higher Mach numbers, which is related to the size of the test section. The integration of a nozzle is a critical step in transitioning from a shock tube to a shock tunnel, facilitating the transformation of high-pressure and high-temperature gas from the shock tube into the high-speed flow required for experiments in the shock tunnel. An example is provided in Figure 2.7 [9], which illustrates the attachment of a nozzle to a shock tube. In the next section, we will draw insights from how these stagnation conditions will be utilized and expanded from equations by Chun-Min Wang [39] offer valuable parallels to the flow conditions we aim to create in our shock tunnel. Additionally, research by John W. Davis et al. [12] provides similar insights into the design and operation of such systems,

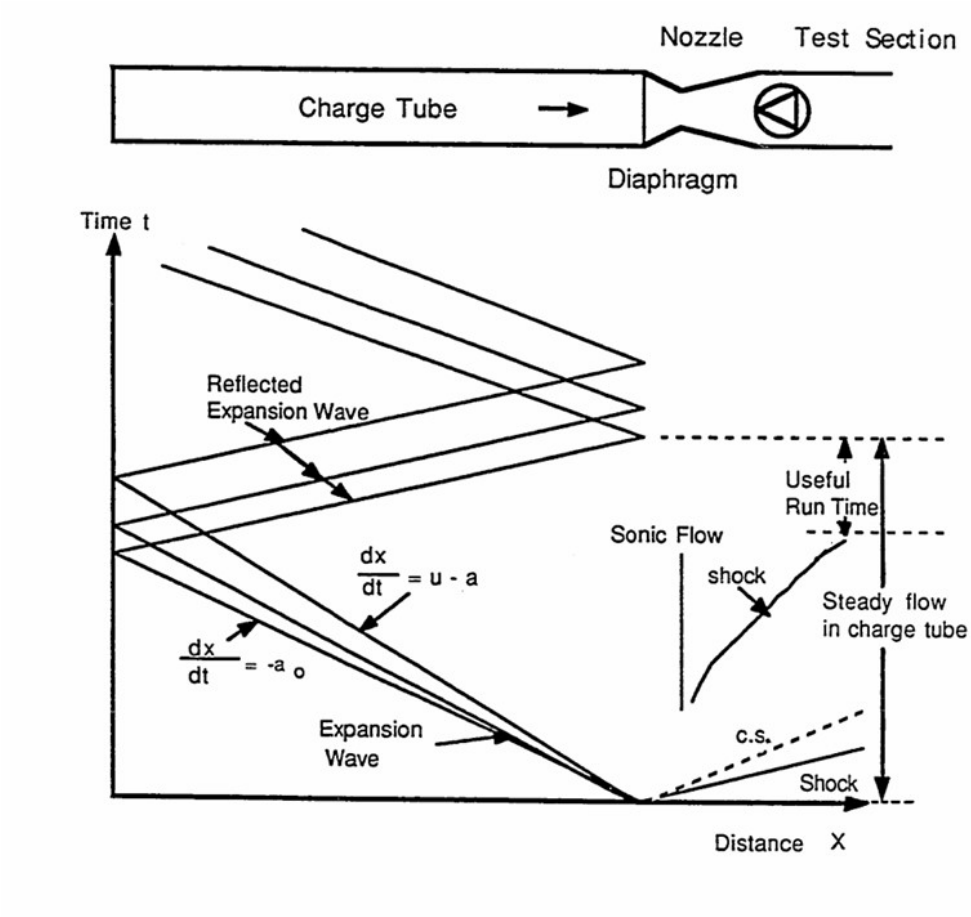


Figure 2.6: Ludwieg Tube Representation [39]

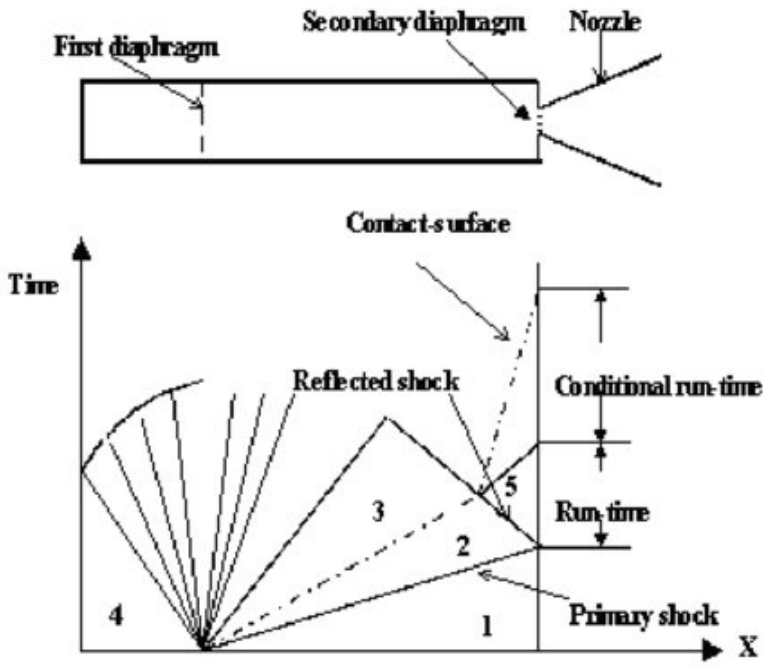


Figure 2.7: (a) Schematic layout of single diaphragm constant-area shock tube and (b) wave (x–t) diagram of the gas flows [9]

which are highly relevant to our shock tube and nozzle integration. By leveraging these studies, we aim to design our facility, ensuring it meets the demanding requirements of high-speed flow experiments.

### *2.3.3 Expansion Loss with Nozzle Performance*

We feed the stagnation conditions from the shocktube through the lossless nozzle. These differ because the upstream Mach number is nonzero. To solve for the flow condition upstream of the nozzle during the shock tunnel cycle, Equations (2.2) and (2.3) are utilized. As shown in Equation (2.4), the ratios of stagnation to total pressure and density are derived from isentropic relations based on the temperature ratio. We know that the ratios of stagnation temperature to total temperature, stagnation pressure to total temperature, and static pressure to total pressure are functions of the tube-to-throat area ratio and the Mach number upstream of the nozzle as in Figure 2.8.

$$\frac{A_{tube}}{A_t} = \left(\frac{D_{\text{tube}}}{D_t}\right)^2 = \frac{1}{M_{\text{up}}}\left(\frac{2}{\gamma+1}\left(1+\frac{\gamma-1}{2}M_{\text{up}}^2\right)\right)^{\frac{\gamma+1}{2(\gamma-1)}}$$

Ratio between stagnation temperature upstream the nozzle and total temperature can be expressed as a function of the Mach number upstream the nozzle.

$$\frac{T_{0,flow}}{T_{tube}} = \left(\frac{1+\frac{\gamma-1}{2}M_{up}^2}{1+\frac{\gamma-1}{2}M_{up}}\right)^2 \tag{2.1}$$

Isentropic relation is used to calculate stagnation pressure to total pressure ratio from stagnation temperature to total temperature ratio.

$$\frac{P_{0,flow}}{P_{tube}} = \left(\frac{a_{0,flow}}{a_{tube}}\right)^{\frac{2\gamma}{\gamma-1}} \tag{2.2}$$

Here, tube values are the stagnation conditions in the shocktube section and will be connected to the nozzle, which will be expanded. Finally, the nozzle test section stagnation temperature ($T_{0,test}$) is calculated and similarly for the nozzle test section pressure ($P_{0,test}$).

We employed an in-house code that puts these equations in work. e solve by providing inputs such as $P_{0,\text{tube}}$ and $T_{0,\text{tube}}$, the stagnation conditions of the shock tube, Additional inputs include the Mach number and test section diameter, which define the area ratio and govern the flow characteristics. We work with ideal gas assumptions and proceed to choose the specific heat ratio and molecular weight of the selected gas, in our case **air**, which calculates the gas constant. Using isentropic flow relations, the function determines temperature, pressure, and area ratios for a given Mach number. We compute the throat diameter based on the test section diameter and area ratio. The function calculates the upstream Mach number, total temperature, and pressure ratios across the tunnel. Finally, it determines the stagnation conditions and Reynolds number, using the static temperature and pressure to find the flow density and dynamic viscosity, thus characterizing the flow properties.

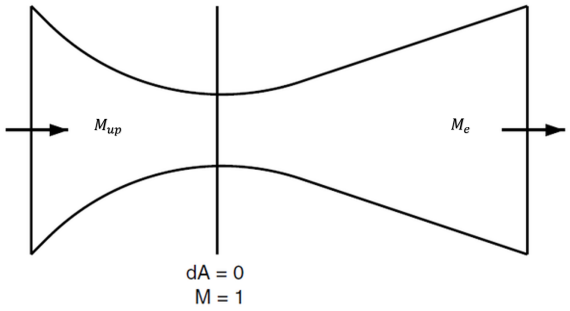


Figure 2.8: $M_{up}$: Location of Upstream Mach

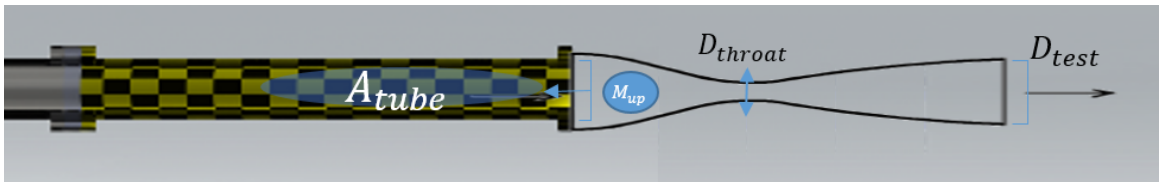


Figure 2.9: Nozzle Integration for our Design

# Chapter 3

# RESULTS

## *3.1 Shock tube calculations*

**Air** is assumed as the test gas. We assume ideal gas equations of state and an inviscid flow, even at high temperatures. The fill gas temperature is maintained at 300 $K$ while allowing the driver pressure, ($P_4$), to vary between 100 to 5000 $psi$. The maximum driver pressure being 5000 $psi$ because it is the structural integrity limit of the pipe. The driven pressure, ($P_1$), is varied between 0.5 to 50 $atm$ (7.5 to 750 psi) minimum and maximum values used in our design. In our setup, we used specific pressure ratios as constraints to achieve desired test conditions. These pressure ratios, denoted as $P_4/P_1$, were carefully selected to ensure the desired flow parameters such as stagnation pressure and temperature. $\frac{P_4}{P_1} > 1$ is another limiting condition. Full scale driver and driven lengths are defined according to Figure 2.1. We aim to investigate how variations in the length of the tube, the pressure in the driver ($P_4$) and driven section ($P_1$) influence the stagnation conditions at the downstream end of the driven tube, as well as the time that these conditions are available.

### *3.1.1 Influence of $P_4$, $P_1$ and Length on Flow Dynamics*

This section provides an example and shows how adjustments in length and pressure settings influence output variables, visually represented in Figures 3.1 for different lengths, building on the initial case from Figure 2.3. In our design, we systematically varied driver and driven pressures and lengths to achieve desired testing conditions, resulting in diverse pressure and temperature profiles along the shock tube, visualized using x-t charts. We observe that test times are predominantly influenced by the shock tube length, despite variations of the pressure in the driver and driven section. As shown in Figure 3.4 ($c$) indicates a dominant influence of shock tube length on overall test duration. These results highlight that while stagnation conditions such as pressure and temperature are critical, the tube length plays

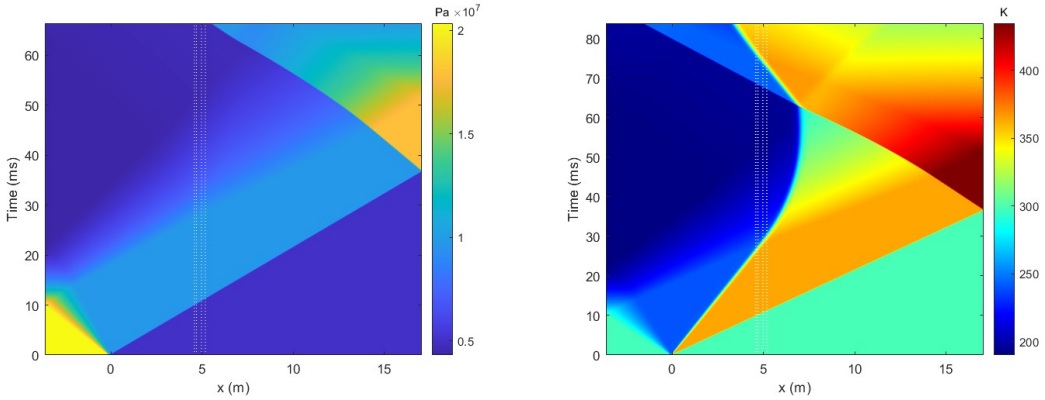


(a) Pressure (b) Temperature

Figure 3.1: Full Length $(P_4) = 3000\ psi$ | $(P_1) = 750\ psi$ [29]

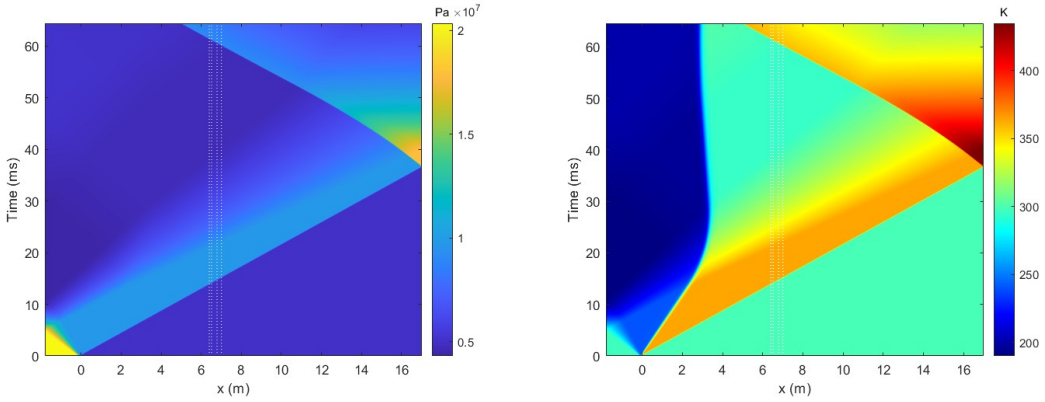


(a) Pressure (b) Temperature

Figure 3.2: Driver Section Halved $(P_4) = 3000\ psi$ | $(P_1) = 750\ psi$ [29]

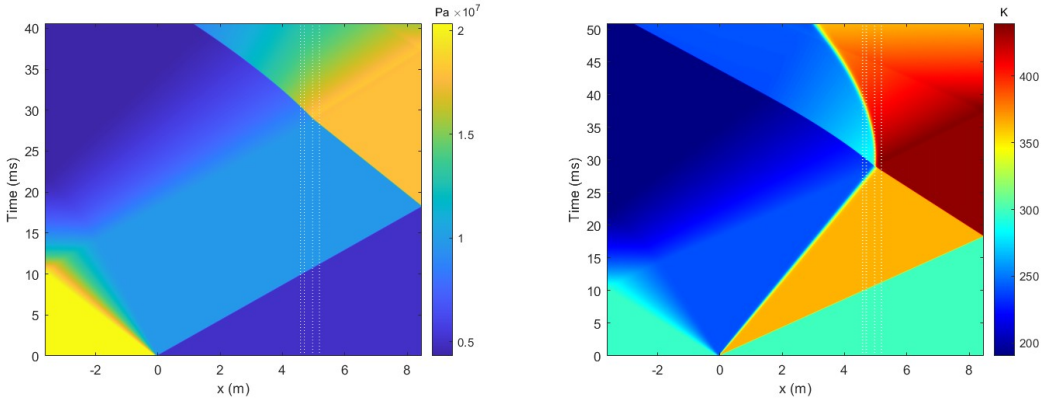


(a) Pressure (b) Temperature

Figure 3.3: Driven Section Halved $(P_4) = 3000\ psi$ | $(P_1) = 750\ psi$ [29]

a more substantial role in determining test times.

Variations in the driven pressure ($P_1$) significantly impacted stagnation pressure and temperature. As depicted in Figure 3.4 ($a$), stagnation pressure was highest at the highest $P_1$ (50 atm), while the greatest stagnation temperature in Figure 3.4 ($b$) was observed at the lowest $P_1$(0.5 atm). This indicates that $P_1$ is crucial in determining stagnation conditions downstream of the shock tube. Lower driven pressures reduced stagnation pressures due to less compression of the driver gas by the shock wave. Higher driven pressures resulted in lower stagnation temperatures.

Elevated driver pressures ($P_4$) increased stagnation pressures by energizing the shock wave, enhancing compression as highlighted in Figures 3.4 (a) and (b). Higher driver pressures also yielded higher stagnation temperatures. In shock tube experiments, higher driver pressures led to shorter test times due to the increased energy imparted to the shock wave, facilitating faster wave propagation. The combined effects are a consequence of pressure ratio variations ( $P_4/P_1$ ).

Summarizing the expected trends using Figure 3.4, we can see the critical importance of both driver and driven pressures in determining the performance characteristics of the shock tube, with stagnation pressures reaching around 0.7 times the maximum pressure ($P_{4,\max}$ = 5000 psi) and stagnation temperatures reaching up to 5 times the ambient temperature

($T_{\text{amb}} = 300$ K) and test time in the range of 3 ms - 16ms. We continue with the Full Length cases as our earlier findings indicated that changes in length do not affect stagnation values. Now we will now expand these these conditions through a lossless nozzle to design a shock tunnel and present the corresponding data outputs.

## *3.2 Adding a Nozzle and Test Section*

### *3.2.1 Trade-offs between test section size and Mach number*

Having obtained the stagnation conditions from the shock tube analysis, we now expand these by attaching a nozzle. A crucial parameter in this context is the upstream Mach number ($M_{up}$), as illustrated in Figure 2.8. Observations from Figure 3.5 indicate that $M_{up}$ increases rapidly with the size of the test section. The relationship between $M_{up}$, test section size, and Mach number reveals practical limits on the achievable size and Mach number in the final facility. This calculation, while independent of the shock tube analysis, underscores the system design limitations. A smaller throat diameter constricts the mass flow, enabling efficient acceleration to the desired high Mach number in the test section. Therefore, careful consideration of $M_{up}$ is essential for optimal performance. To determine the upstream Mach limit for a given driven tube, we equate the mass flow rate in the driven tube to that at the nozzle throat, based on the isentropic area relation. This ensures that the driver tube mass flow rate matches the nozzle throat mass flow rate. Maintaining a low $M_{up}$ helps achieve stable flow conditions by maximizing total pressure and temperature, with $M_{up} \leq 0.1$ typically required. For our test setup, the limit for $M_{up}$ is 0.05 [16].

In Figure 3.6 ($a$) and ($b$), we explore the effect of test section diameter on stagnation pressure ($P_{0,\text{test}}$) and stagnation temperature ($T_{0,\text{test}}$). Assuming a lossless nozzle, we account for the non-isentropic nature of shockwave reflections, which results in a decrease in total pressure due to the irreversible shock processes. The reflected shock wave compresses and heats the flow, increasing entropy and leading to a reduction in total pressure downstream of the shockwave, that expands through the nozzle. However, a non-zero upstream Mach number reduces both stagnation pressure and temperature within the test section ($P_{0,\text{test}}$ and $T_{0,\text{test}}$), as described in Equations (2.3) and (2.4). To mitigate significant re-

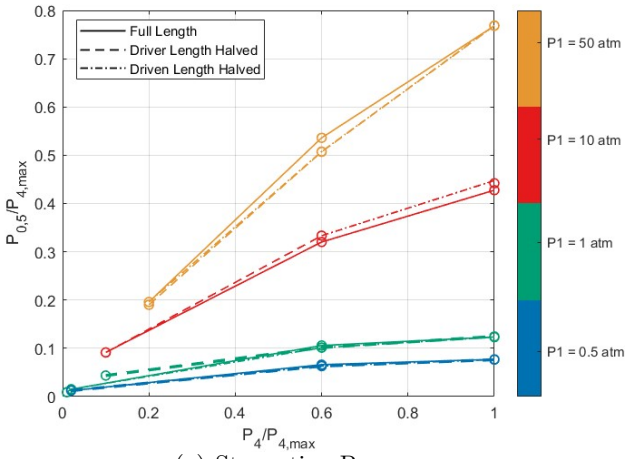


(a) Stagnation Pressures

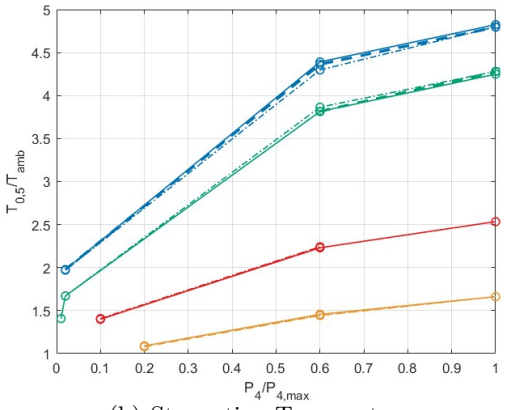


(b) Stagnation Temperatures

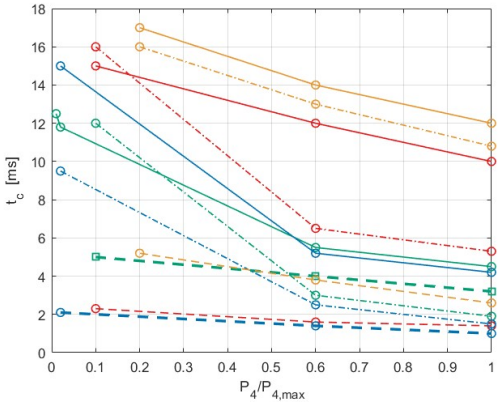


(c) Test Time

Figure 3.4: $P_{0,5}$, $T_{0,5}$ and $t_c$ for Test Cases subjected to Various Lengths, $P_4$ - 100psi to 5000 psi and $P_1$ - 0.5 atm to 50 atm.

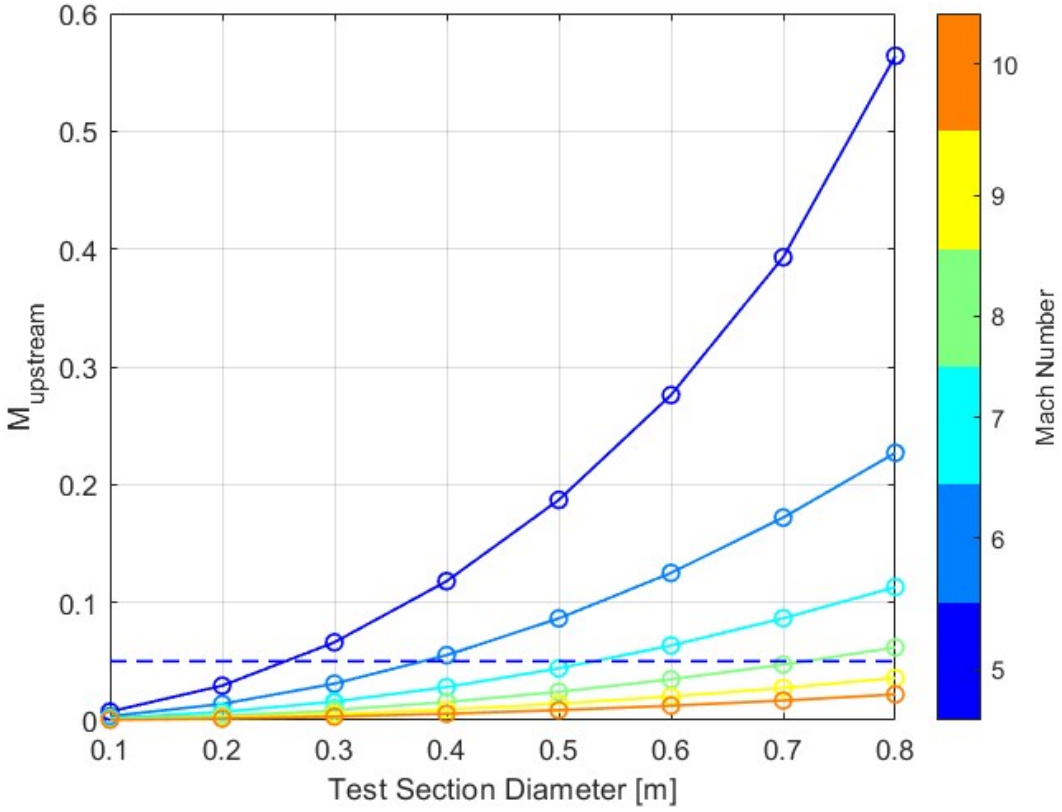


Figure 3.5: Upstream Mach Test Section ($M_{up}$) for M = 5 to 10, as a function of Test Diameter [m]

ductions in stagnation pressure and temperature, it is crucial to maintain a small upstream Mach number. Thus, the throat diameter should be smaller than the pipe diameter. By analyzing these reductions relative to the upstream Mach number ($M_{\text{up}}$), we can optimize the test section size, minimizing the reduction in these losses in stagnation pressures and temperatures while ensuring efficient flow conditions.

### *3.2.2 Variation in test section conditions at Mach* 7

After obtaining the outputs using the nozzle, our focus shifted to observing variations in pressures within the shock tube and exploring the trade-offs between these pressures and the resulting stagnation conditions ($P_{0,\text{test}}$) and ($T_{0,\text{test}}$). We previously noted that

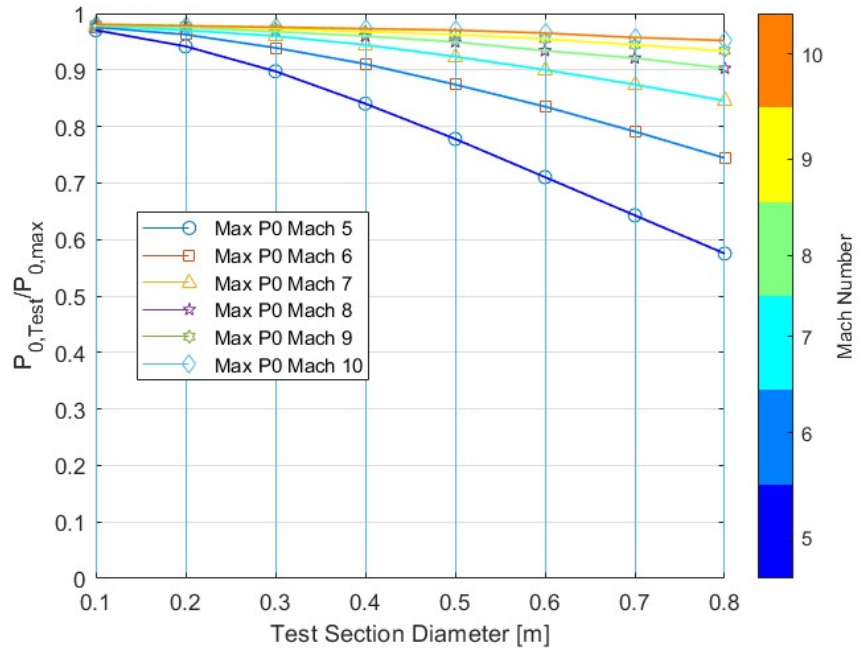


(a) Stagnation Pressures

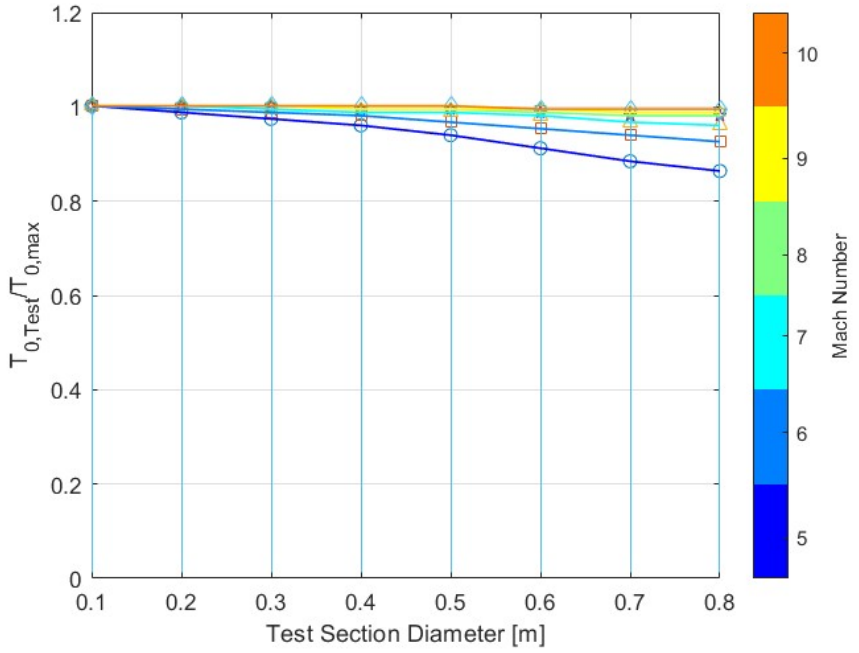


(b) Stagnation Temperatures

Figure 3.6: Test Cases for $P_{0,test}$ and $T_{0.test}$ variation with Test Section Diameter

Mach number has a marginal effect on the test conditions, and we ensured that they meet the stability criteria for the upstream Mach number ($M_{up}$). Based on our analysis, we determined that a test section diameter of 0.3 meters and Mach 7 would be a reasonable balance to work with. **From now , we will be proceeding only with a test section diameter of 0.3 meters.** It is important to note that the stagnation pressure ($P_{0,\text{test}}$) and stagnation temperature ($T_{0,\text{test}}$) in the test section values primarily exhibit sensitivity to the driven pressure as indicated in Figure 3.7. This sensitivity is rational, as it is independent of Mach number. In contrast, Mach number is more closely related to a reductions in **stagnation** pressure and temperature, which, in turn, are associated with the size of the test section. Similar to stagnation pressure and temperature, Reynolds number and enthalpy are primarily sensitive to driven pressure. There is a clear and observable trade-off between Reynolds number and enthalpy, with an increase in driven pressures leading to a reduction in enthalpy but an increase in Reynolds number as depicted in Figure 3.8.

### *3.3 Variation in potential tunnel capabilities across a range of Mach numbers*

The range of Reynolds numbers and enthalpies achievable for the full range of $P_1$ and $P_4$ are now investigated for a range of test section Mach numbers. We acknowledge that the upstream Mach number for the Mach 5 case is marginally above the 0.05 target threshold for these calculations, which is not ideal, but they still serve to illustrate the potential range of conditions achievable with the available pipes and chosen design.

The design of our shock tunnel allows for a broad range of Reynolds numbers, spanning from $10^6$ to $10^8$ $m^{-1}$, with the maximum Reynolds number achievable for a case of $P_4$ of 5000 $psi$ and $P_1$ of 750 $psi$. The tunnel also exhibits a wide range of enthalpies, from 0.3 to 1.6 $MJ/kg$, and maximum achievable enthalpy for a case of $P_4$ of 5000 $psi$ and $P_1$ of 7.5 $atm$. Operating at the edges of these ranges would require careful monitoring and control of the driver and driven pressures ($P_1$ and $P_4$) to ensure stable and reliable operation.

Additionally, operating at higher Mach numbers may lead to diminishing returns in terms of achievable Reynolds numbers and enthalpies, as the flow becomes more compressible and the energy exchange less efficient. The notable sensitivity of the Reynolds number to driven pressure underscores the significant impact of driving conditions on flow characteristics

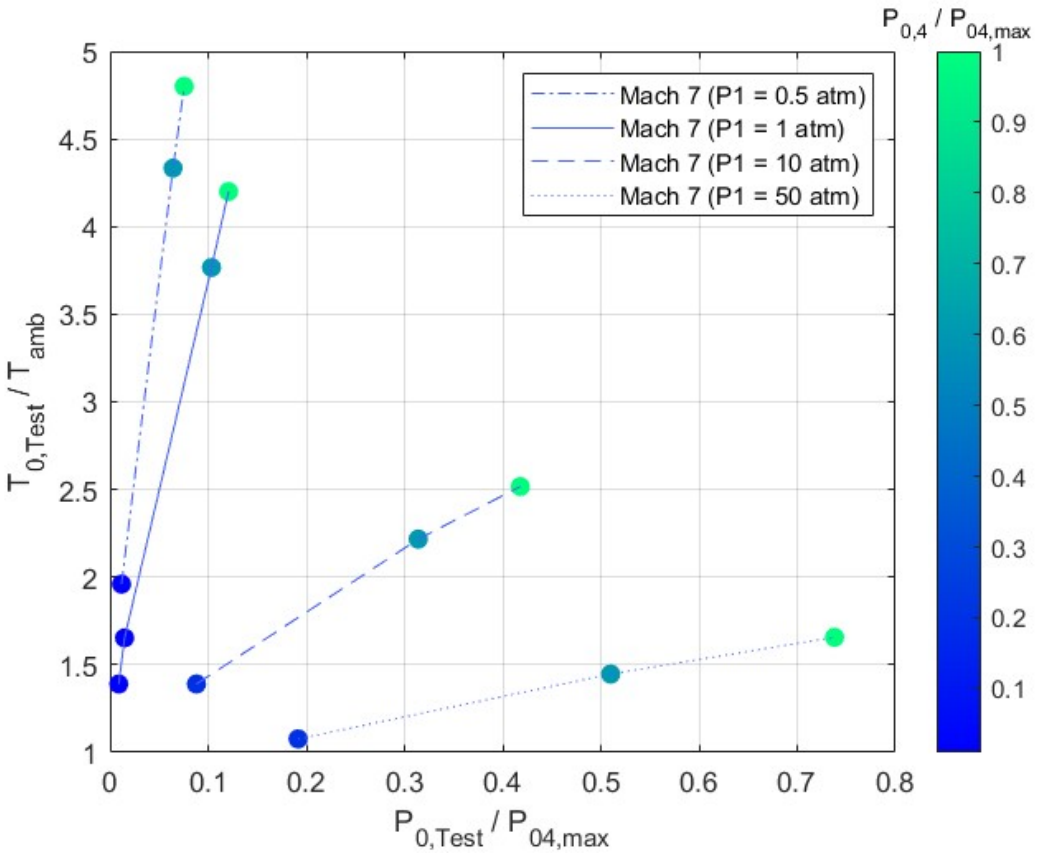


Figure 3.7: $P_0$ vs $T_0$ at Mach 7

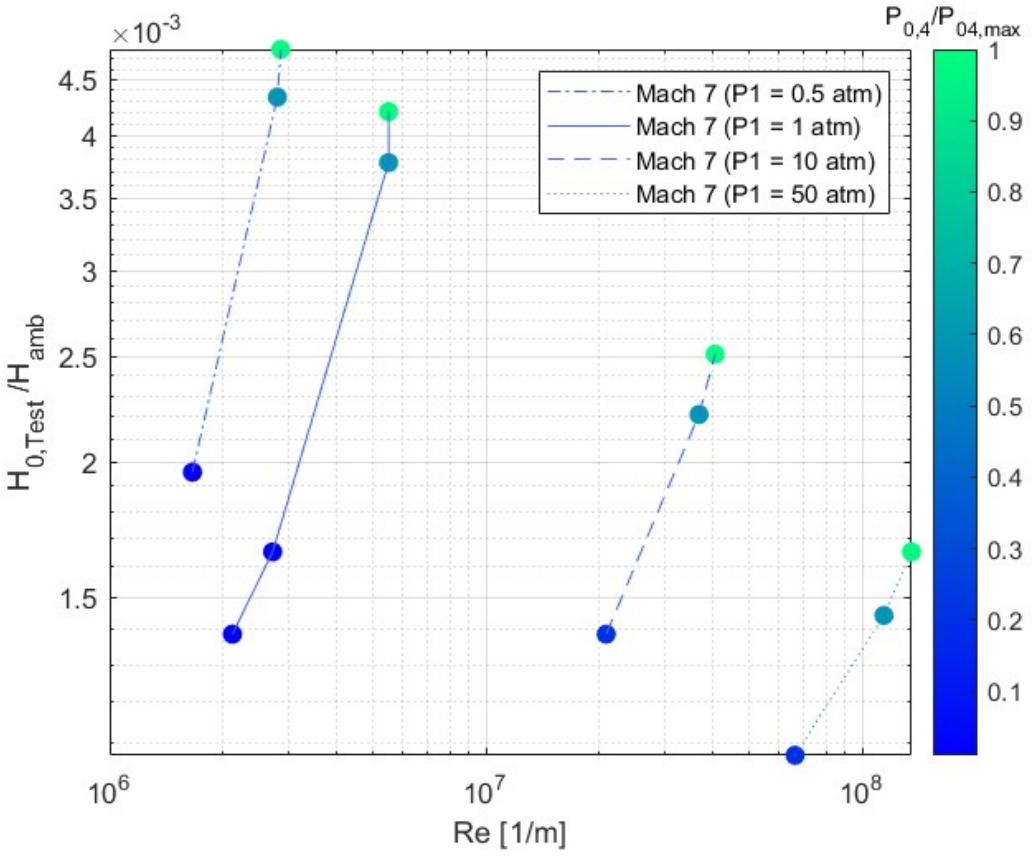


Figure 3.8: Re vs $H_0$ at Mach 7

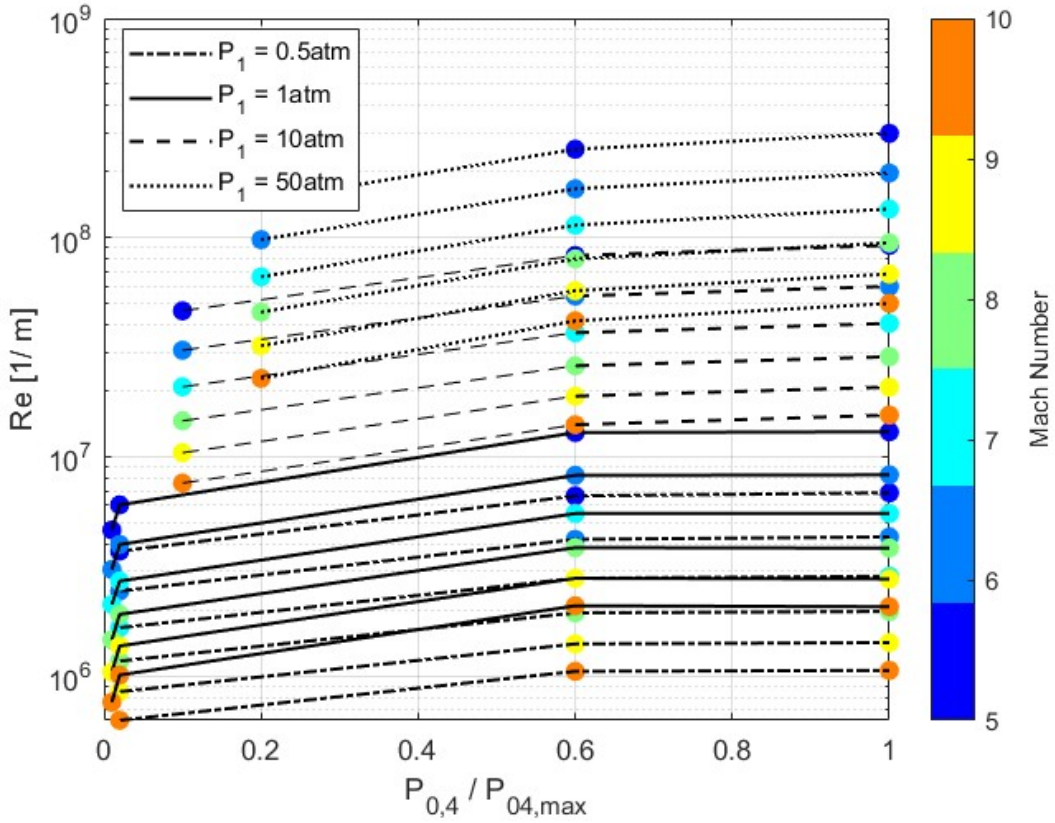


Figure 3.9: Re vs Driver Pressure for for M = 5 to 10

as observed in Figure 3.9. Similarly in Figure 3.10, the total enthalpy decreases with an increase in driven pressure indicating a clear trade-off with $P_1$.

The static temperature in the test section decreases as the Mach number increases. Gas condensation must be avoided in the test section of the final design so that its properties are more clearly understood. As a result, the variation in the test section static temperature is explored as a function of the full shock tunnel setup parameters (Mach number, $P_4$ and $P_1$) in Figure 3.11. To ensure the flow temperature exceeds the condensation point of 60 K, we may need to either reduce the Mach number, heat the gas, or limit the operation to the higher driver pressures or lower driven pressures where condensation is less likely.

Based on our analysis, we recommend a Mach number that works reasonably well for a

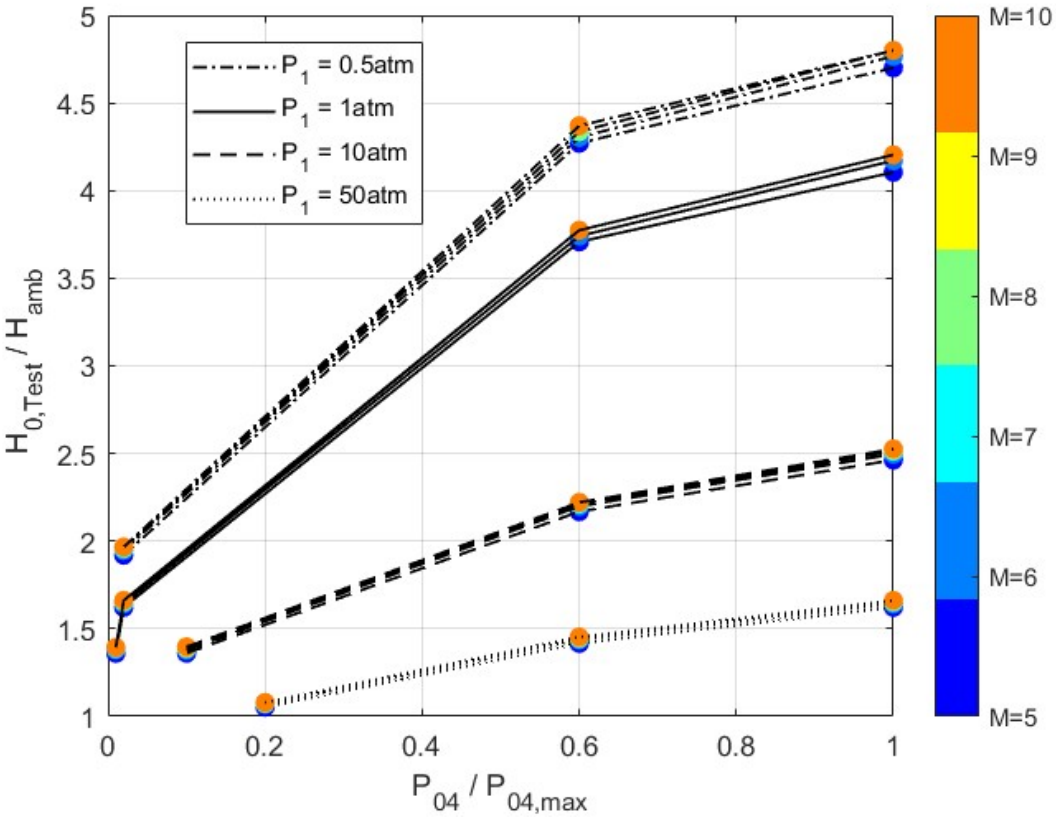


Figure 3.10: Enthalpy Number vs Driver Pressure for M = 5 to 10

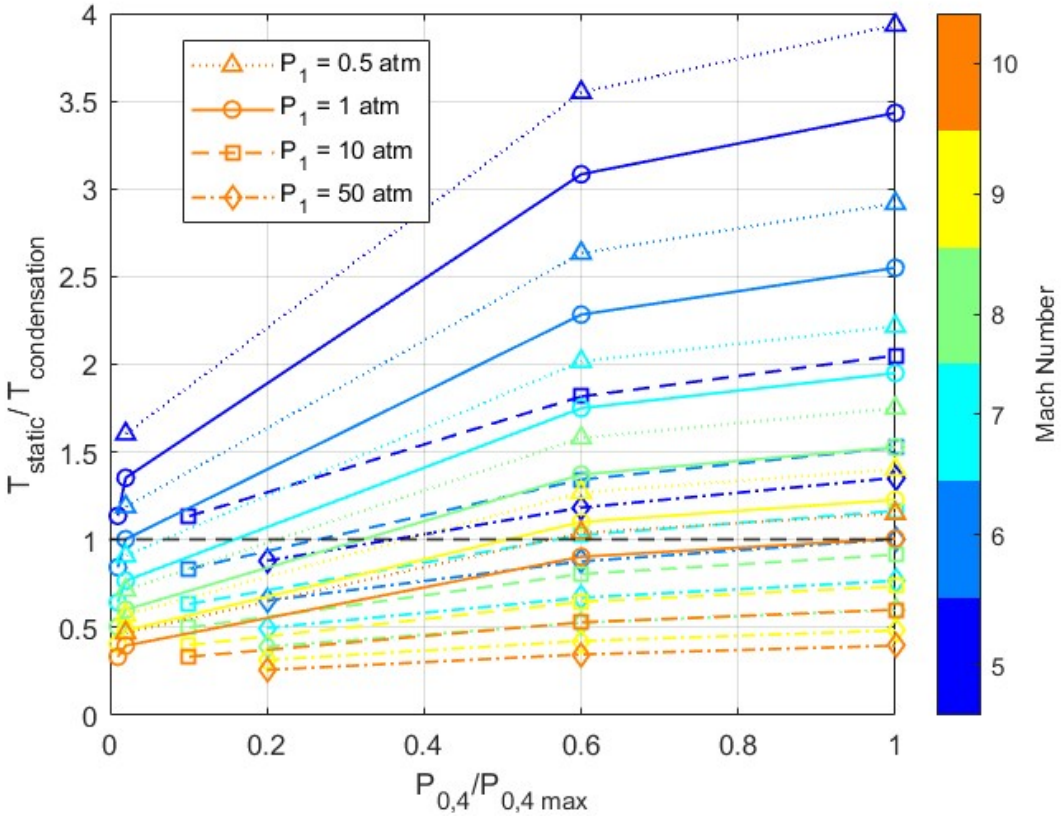


Figure 3.11: Statics Temperature ($T_{static}$) in Test Section vs Driver Pressure

range of $P_1$ and $P_4$ values for which we can operate the tunnel while avoiding condensation. For example, we could work at a Mach number of 6 to 8 and a range of $P_1$ with (0.5 $atm$ - 1 $atm$) and $P_4$ (1000 $psi$ or above) that ensures the flow temperature remains above 60 K , which is chosen as the liquefaction of air for safety measures [42].

### *3.4 Contrasting Designs: UW Shock Tunnel vs UW Ludiweg Tube Configurations*

The test section conditions achievable with the above shock tunnel configuration are compared to those that can be obtained for a Ludwieg tube configuration involving the use of just the driven section pipe. The same gas (air) and maximum pressures are assumed, and the gas is at ambient conditions during fill. The test section size for both facilities is 0.3

meters. Full details of the Ludweig tube configuration were given in Section 2.3.1 and the design was conducted by Marvin Bok [27]. The Ludweig tube tests (without heating) are conducted for Mach 5, 7, and 10.

In considering the choice between Ludweig tubes and shock tunnels for hypersonic research, it becomes evident that specific requirements play a pivotal role, particularly concerning the desired trade-off between Reynolds number and enthalpy, as well as the balance between stagnation pressure and temperature. As shown in figures 3.12 ($a$) and ($b$), this trade-off is significant as a higher Reynolds number often necessitates a compromise on enthalpy. Nonetheless, the close ranges observed for each Mach number ensure a degree of flexibility for such compromises. For outputs (our facilities) necessitating a broader range of Reynolds numbers, the Ludweig tube configuration may be favored, particularly at lower Mach numbers. Conversely, if a wider range of enthalpies is imperative, especially at higher Mach numbers, the shock tunnel configuration may be more advantageous.

Contrasting test times for the two facilities are shown in Figure. 3.13. The shock tunnel configuration yields a relatively lower range of test times, with the best-case scenario ($P_4 =$ 1000 psi and $P_1 = 50$ atm) ranging from 12 to 16 $ms$. In contrast, the Ludwieg tube exhibit test times, spanning from 95 to 98 $ms$. This trend is likely to be true, in general, because the shock tunnel operates with significantly higher pressures and temperatures, leading to shorter durations of steady test conditions. Conversely, the Ludwieg tube is designed to achieve longer test times by maintaining a quasi-steady flow through a different mechanism that relies on the controlled release of high-pressure gas from a reservoir, allowing for more extended periods of stable flow conditions. This fundamental difference in operation modes contributes to the observed variation in test times between the two facilities.

## *3.5 Comparative Analysis of the shock tunnel design with other reflected shock tunnels*

This comparative study evaluates the high enthalpy replication capabilities of our shock tunnel facility in comparison to other leading facilities as indicated in Table 3.1 [18]. Unlike table 1.1, table 3.1 emphasise is on stagnation conditions and test times for all types of hypersonic facilities in particular, invoking a more diverse view. We have also incorporated

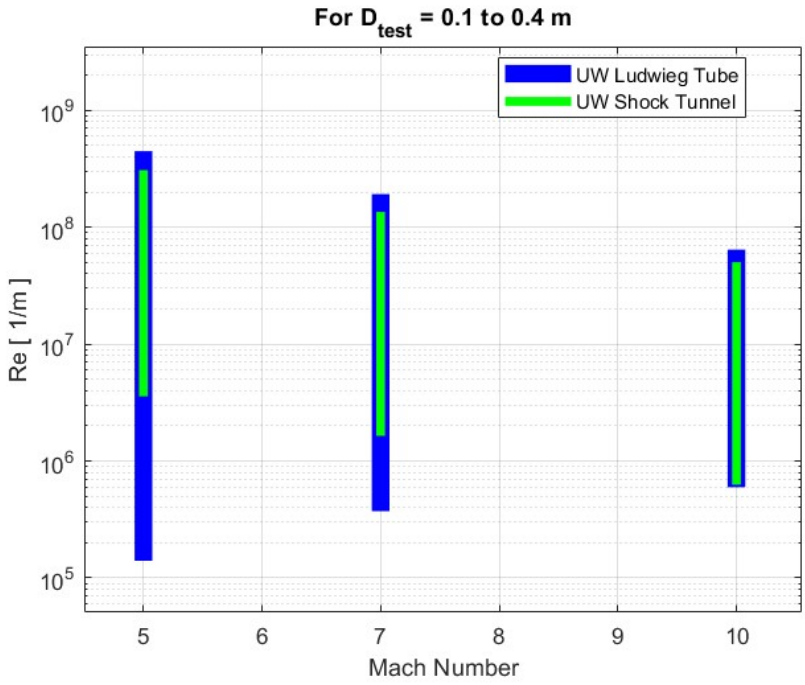


(a) Reynolds Number

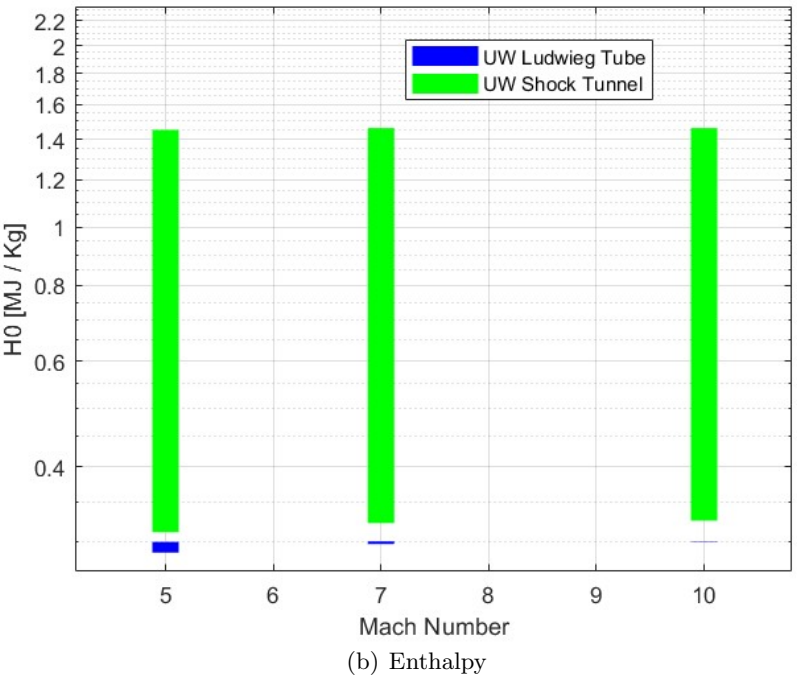


(b) Enthalpy

Figure 3.12: $Re$ & $H_0$ for UW Ludwieg Tube [27] vs. UW Shock Tunnel

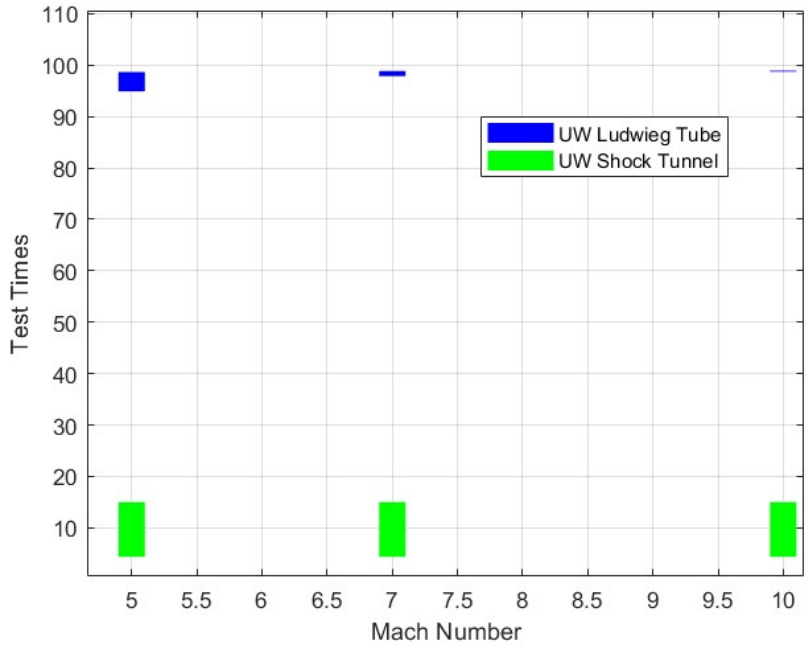


Figure 3.13: Ludwieg Tube vs. UW ShockTunnel Test Time

an additional set of Reflected Shock Tunnel Facilities in the table such as SANDIA [25], STEVENS [33] and HyperTERP [5], allowing us to for a detailed comparison.

Our facility excels in pressure capabilities, for a Mach of 10, offering a maximum pressure ($P_{0,test}$) of 26 MPa . This exceeds the capacities of well-known facilities such as the Sandia Tunnel (18 MPa), HyperTERP (2 MPa), and JF12 (3.5 MPa). Additionally, our facility achieves a maximum temperature ($T_{0,test}$) of 1500 K, surpassing the capabilities of the HyperTERP (Maryland) and Stevens Shock Tunnel, as indicated in Table 3.1. We conducted a detailed comparison with the other Reflected Shock Tunnels, as shown in Figure 3.14 using [18]. The test time ($t_c$) for our facility of 3-16 $ms$ as depicted in figures 3.14 is competitive and falls within the range of test times offered by other reflected shock tunnel facilities in particular. It seems to be on par only with the LENS I facility that spans from 2- 18 $ms$. This comparison underscores the favorable test times achieved by our facility, aligning closely with those of LENS I. It is noteworthy that we are able to be flexible with a good range from **3 to 16** $ms$, which is the second largest range present. We have ex-

Table 3.1: Characteristics of Some Reflected Shock Tunnels [18]

| Facility type | Facility | $P_{0,\max}$, MPa | $T_{0,\max}$, K | Test time | Test Dia, m |
|---|---|---|---|---|---|
| Reflected shock tunnels | TH2 | 63 | 7400 | 2 ms–10 ms | 0.586 |
| | JF12 | 3.5 | 2500 | 100 ms–150 ms | 1.5–2.5 |
| | T4 | 90 | 7540 | 0.5 ms–5 ms | 0.135–0.375 |
| | T5 | 85 | 10000 | 1 ms–2 ms | 0.3 |
| | HEG | 90 | 9900 | 1 ms–6 ms | 0.43–0.88 |
| | HIEST | 150 | 10000 | 2 ms- 5 ms | 0.8–1.2 |
| | **UW Shock Tunnel Design** | **26** | **1500** | **3 ms - 16 ms** | **0.3** |
| | Sandia | 18 | 3700 | 2 ms - 3 ms | 0.5 |
| | Stevens | - | - | 1 ms - 4 ms | 0.610 |
| | HyperTERP | 2 | 1400 | 2.5 ms - 8 ms | 0.305 |
| | HYPULSE | 3000 | 8000 | 3 ms - 7 ms | 0.3 |
| | LENS I | 200 | 7000 | 2 ms - 18 ms | 0.5–1.2 |

cluded JF12 from our analysis, as it has test times greater than **150** $ms$. Even though it is a shock tunnel, it operates on a completely different principle, which is defined as the Backward-running Detonation Driver. It uses a detonation process, where the shock wave propagates **backward**, compressing the driver gas to a high pressure and has an extremely large testing section, around 265 meters.

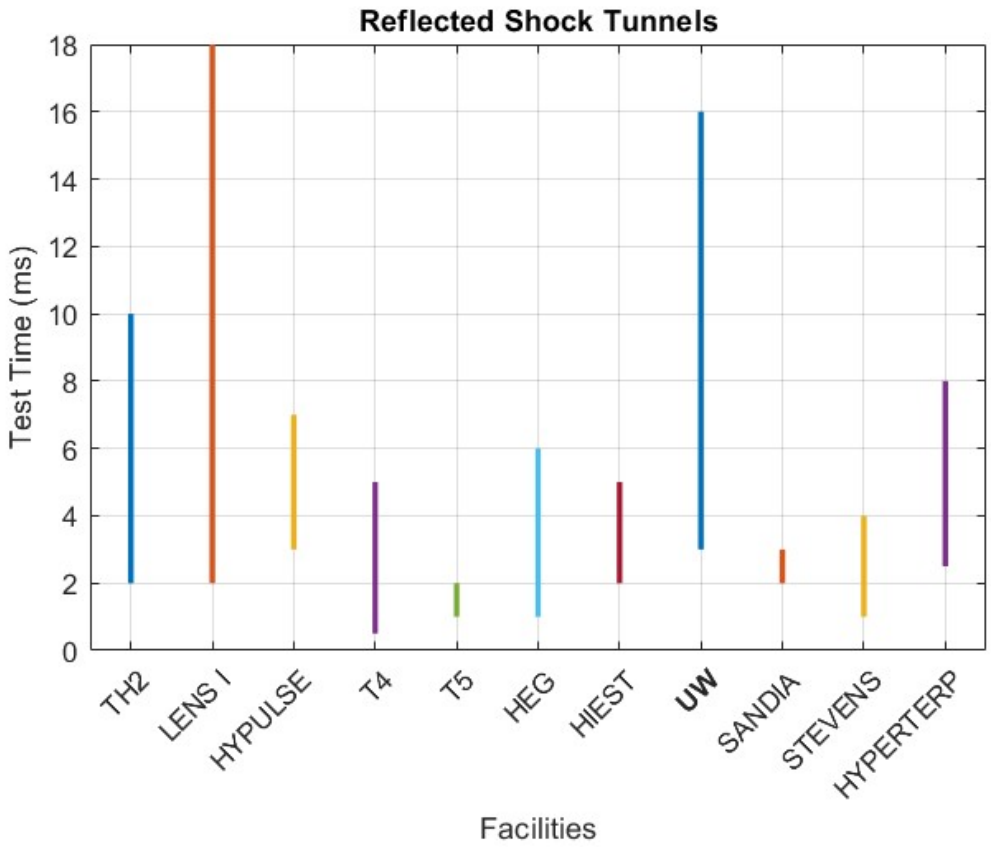


Figure 3.14: Test Time Comparison With Other RST Facilities [18]

# Chapter 4

# CONCLUSION

The design of a hypersonic reflected shock tunnel (RST) using available pipes within the UW AA department has demonstrated significant capabilities in achieving precise and high-performance test conditions. This study analyzed variations in pressure, temperature, and test times across Mach numbers from 5 to 10, shock tube length, and pressures in the driver ($P_4$) and driven sections ($P_1$), utilizing the WISTL code [29] from the University of Wisconsin and incorporating nozzle expansion into the test section.

In our design, stagnation pressures reached up to 26 MPa and temperatures up to 1500 K. Test times of up to 16 ms were achieved with lower driver pressures ($P_4 \approx 500$ psi) and higher driven pressures ($P_1 \approx 750$ psi). The shortest test time of 3 ms was achieved by using higher driver pressures ($P_4 \approx 1000$ psi) and lower driven pressures ($P_1 \approx 75$ psi). The final test section diameter was set at 0.3 meters, which was ideal for limiting the upstream Mach number of the nozzle (maintaining the validity our assumptions). Additionally, a full-length tube configuration was chosen to provide a wider range of test times.

To avoid condensation and ensure reliable flow dynamics, the final conditions were selected based on maintaining flow temperatures above 60 K. This was achieved by carefully controlling $P_1$ within a range of 7.5 to 150 psi and $P_4$ at values greater than 1000 psi. These conditions prevented gas condensation in the test section. This range allows for Reynolds numbers from $10^6$ to $10^8$ $m^{-1}$ and enthalpies varying from 0.3 to 1.6 MJ/kg. An optimal Mach number range of 6 to 8 was identified, taking into consideration the upstream Mach number and the static temperature limits and offering the best balance between achieving high Reynolds numbers of $10^7$ to $10^8$ $m^{-1}$ and high enthalpy levels of 0.8 to 1.3 MJ/kg.

Compared to other facilities, our hypersonic RST achieves a broad range of Reynolds numbers and enthalpies with precise control over test conditions, similar to other advanced reflected shock tunnels. While RSTs excel in providing extended test times and flexible

Reynolds nmber and enthalpies, Ludweig tubes offer longer test durations with higher repetition rates, making them ideal for different types of high speed flows. This makes our RST design particularly well-suited for in-depth, high-performance research applications.

In conclusion, our hypersonic RST design offers flexible and high-performance test conditions, making it suitable for diverse hypersonic research applications. This comprehensive approach has resulted in a reflected shock tunnel design that is comparable to other advanced facilities.

# BIBLIOGRAPHY

[1] Y.M. Abul-Huda and M. Gamba. Flow characterization of a hypersonic expansion tube facility for supersonic combustion studies. *Journal of Propulsion and Power*, 33:1504–1519, 2017.

[2] Jr. Anderson, John D. *Fundamentals of Aerodynamics*. McGraw-Hill Education, 6th edition, 2015.

[3] Jewel B. Barlow, William H. Rae Jr., and Alan Pope. *Low-Speed Wind Tunnel Testing*. John Wiley & Sons, 3rd edition, 2016.

[4] A. Ben-Yakar and R.K. Hanson. Characterization of expansion tube flows for hypervelocity combustion studies. *Journal of Propulsion and Power*, 18:943–952, 2002.

[5] Cameron S. Butler and Stuart J. Laurence. Hyperterp: A newly commissioned hypersonic shock tunnel at the university of maryland. 2020.

[6] M. F. Campbell, T. Parise, A. M. Tulgestke, R. M. Spearrin, D. F. Davidson, and R. K. Hanson. Strategies for obtaining long constant-pressure test times in shock tubes. *Unknown*, Unknown.

[7] Calspan-UP Research Center. Large energy national shock tunnel (lens) description and capabilities. 12 1990. Accession Number: 5690, Publication Date: Dec 01, 1990, Descriptors, Keywords: Energy National Shock Tunnel LENS, Pages: 58, Cataloged Date: May 25, 1995, Document Type: HC, Number of Copies In Library: 1, Record ID: 30053.

[8] R. S. M. Chu, C. Y. Tsai, and R. J. Bakos. Driver gas contamination in a detonation-driven reflected-shock tunnel. *Shock Waves*, 13:367–380, 2004.

[9] Chi Chun. Real gas effect on transient flow phenomena in a reflection shock tunnel. *Journal of Flow Visualization and Image Processing*, 12(2):175–195, 2005.

[10] Peter Collen, Luke J. Doherty, Suria D. Subiah, Tamara Sopek, Ingo Jahn, David Gildfnd, Rowland Penty Geraets, Rowan Gollan, Christopher Hambidge, Richard Morgan, and Matthew McGilvray. Development and commissioning of the t6 stalker tunnel. *Unknown*, 2021. Received: 31 December 2020 / Revised: 7 July 2021 / Accepted: 19 August 2021.

[11] M. Colombo, M. di Prisco, and P. Martinelli. A new shock tube facility for tunnel safety. *Society for Experimental Mechanics*, 2010:1–10, 2010.

[12] John W. Davis and Hal S. Gwin. Feasibility studies of a short duration high reynolds number tube wind tunnel. Technical report, NASA George C. Marshall Space Flight Center, Huntsville, Alabama, n.d.

[13] A. Dufrene, M. Sharma, and J.M. Austin. Design and characterization of a hypervelocity expansion tube facility. *Journal of Propulsion and Power*, 23:1185–1193, 2007.

[14] Malte Estorf, Rolf Radespiel, Steven P. Schneider, and Stefan Hein. Surface-pressure measurements of second-mode instability in quiet hypersonic flow. In *46th AIAA Aerospace Sciences Meeting and Exhibit*, 2008.

[15] V.M. Fomin, A.M. Kharitonov, A.A. Maslov, A.N. Shiplyuk, V.V. Shumskii, M.I. Yaroslavtsev, and V.I. Zvegintsev. Hypersonic short-duration facilities for aerodynamic research at itam, russia. In *Experimental Methods of Shock Wave Research*, pages 315–346. Springer, 2016.

[16] Mark Gragston, Kirk Davenport, Farhan Siddiqui, Nicholas Webber, Cary D. Smith, Phillip A. Kreth, and John D. Schmisseur. Design and initial characterization of the utsi mach 7 ludwieg tube. In *AIAA 2023-1457, Session: Design, Construction, or Characterization of New or Modified Ground Test Facilities I*, Jan 2023.

[17] G. Grossir, Z. Ilich, S. Paris, and O. Chazot. Theoretical considerations to extend the operational map of the vki longshot hypersonic wind tunnel. In *32nd AIAA Aerodynamic Measurement Technology and Ground Testing Conference*, 2016.

[18] Sangdi Gu and Herbert Olivier. Capabilities and limitations of existing hypersonic facilities. *Shock Wave Laboratory, RWTH Aachen University, Templergraben 55, 52062, Aachen, Germany*, 3 2020.

[19] Klaus Hannemann, Jan Martinez Schramm, and Sebastian Karl. Recent extensions to the high enthalpy shock tunnel göttingen (heg). *Journal Name*, 2020. This might be a technical report or conference paper, not published in a journal.

[20] Klaus Hannemann, Jan Martinez Schramm, and Sebastian Karl. Recent Extensions to the High Enthalpy Shock Tunnel Göttingen (HEG). *German Aerospace Center*, unknown.

[21] Michael S. Holden. A preliminary study associated with the experimental measurement of the aero-optic characteristics of hypersonic configurations, 1992.

[22] H. Hornung. Performance data of the new free-piston shock tunnel at GALCIT. *Graduate Aeronautical Laboratories, California Institute of Technology*, XXXX.

[23] Zonglin Jiang and Hongru Yu. Experiments and development of the long-test-duration hypervelocity detonation-driven shock tunnel (lhdst). *Journal Name*, Volume(Issue), Year.

[24] Balaram Kundu. Existence of subsonic flow in divergent section adjacent to throat of a convergent-divergent nozzle for actual flow. *Journal of Applied Fluid Mechanics*, 11(2):353–359, 2018.

[25] Kyle P. Lynch, Thomas Grasser, Paul Farias, Kyle A. Daniel, Russell Spillers, Charley Downing, and Justin L. Wagner. Design and characterization of the sandia free-piston reflected shock tunnel. *Sandia National Laboratories*.

[26] D. Marren and J. Lafferty. The aedc hypervelocity wind tunnel 9. In *Advances in Hypersonic Test Facilities*, pages 467–478. 2002.

[27] Marvin. Uw ludwieg tube: Marvin's work. Unpublished manuscript, 2023. Personal communication.

[28] M. Mills. Hypersonic test capabilities in tunnels b and c at aedc's von karman facility. In *53rd AIAA Aerospace Sciences Meeting*, 2015.

[29] J. G. Oakley and R. Bonazza. xt.exe software. Wisconsin Shock Tube Laboratory (WiSTL), Madison, WI, 2004.

[30] Laura A. Paquin, Shaun N. Skinner, and Stuart J. Laurence. Hypersonic boundary-layer disturbances on a cooled, slender cone at mach 6. 2019.

[31] Petersen Research Group, Texas A&M University. Shock-tube physics.

[32] Bryan Schmidt. Galcit 6-inch shock tube. TA: Ae 104b, Lab: Ludwieg Tube, 2013. Phone: 419.681.6128, Email: bsschmid@caltech.edu.

[33] D. Shekhtman, A. Hameed, B. A. Segall, A. R. Dworzanczyk, and N. J. Parziale. Initial shakedown testing of the stevens shock tunnel. *Stevens Institute of Technology*.

[34] D. Shekhtman, M. A. Mustafa, N. J. Parziale, W. M. Yu, and J. M. Austin. Krypton tagging velocimetry (ktv) investigation in the caltech t5 reflected-shock tunnel. *Stevens Institute of Technology, Hoboken, NJ 07030, USA*, unknown.

[35] Michael Smart, Ray Stalker, Richard Morgan, and Allan Paull. Title of the paper. *Journal Name*, 2019.

[36] Hideyuki Tanno, Tomoyuki Komuro, Kazuo Sato, and Katsuhiro Itoh. Wind tunnel test comparison between jaxa-hiest and onera-s4ma with hyflex lifting-body. *Journal Name*, Year.

[37] The Chair. Hypersonic shock tunnel (TH2). Research Overview, 2022. Available online at https://www.academics.com/research/experimental-facilities/hypersonic-shock-tunnel-th2.

[38] Ching-Yi Tsai, Randy Chue, Clay Nicholson, and Jason Tyll. Hypervelocity capability of hypulse shock tunnel for radiative heat transfer measurements at lunar reentries. 2020.

[39] Chun-Min Wang. Transonic flow of a supersonic ludwieg wind tunnel, 1989.

[40] Shengkai Wang. *SHOCK TUBE / LASER ABSORPTION STUDY OF ALDEHYDES KINETICS*. PhD thesis, Ph.D. thesis, Advisor: Ronald K. Hanson, 9 2016.

[41] Shengkai Wang, David F. Davidson, and Ronald K. Hanson. *Shock Tube Techniques for Kinetic Target Data to Improve Reaction Models*, chapter 3. Elsevier, 2015.

[42] P.P. Wegener and L.M. Mack. Condensation in supersonic and hypersonic wind tunnels. Jet Propulsion Laboratory, California Institute of Technology, 1960.

[43] Xiuqi Yang. Ludwieg tube driven aerospike nozzle cold flow. University of Washington, Seattle, WA 98195-2400. William E. Boeing Department of Aeronautics & Astronautics.